Atmospheric Models of red giants with massive scale NLTE

C.I. Short

Department of Astronomy & Physics and Institute for Computational Astrophysics, Saint Mary's University, Halifax, NS B3H 3C3

ishort@ap.stmarys.ca

P.H. Hauschildt

Hamburger Sternwarte, Gojenbergsweg 112, 21029 Hamburg, Germany

phauschildt@hs.uni-hamburg.de

ABSTRACT

We present plane-parallel and spherical LTE and NLTE atmospheric models of a variety of stellar parameters of the red giant star Arcturus (α Boo, HD124897, HR5340) and study their ability to fit the measured absolute flux distribution. Our NLTE models include tens of thousands of the strongest lines in NLTE, and we investigate separately the effects of treating the light metals and the Fe group elements Fe and Ti in NLTE. We find that the NLTE effects of Fe group elements on the model structure and F_λ distribution are much more important than the NLTE effects of all the light metals combined, and serve to substantially increases the violet and near UV F_λ level as a result of NLTE Fe over-ionization. Both the LTE and NLTE models predict significantly more flux in the blue and UV bands than is observed. We find that within the moderately metal-poor metallicity range, the effect of NLTE on the overall UV flux level *decreases* with decreasing metallicity. These results suggest that there may *still* be important UV opacity missing from the models. We find that models of *solar metallicity* giants of similar spectral type to Arcturus fit well the observed flux distributions of those stars from the red to the near UV band. This suggests that the blue and near UV flux discrepancy is metallicity dependent, increasing with decreasing metallicity.

Subject headings: stars: atmospheres, late-type, individual (alpha Boo)—radiative transfer—line: formation

1. Introduction

Because red giant stars are relatively bright and more numerous than other luminous stars, they serve as chemical abundance tracers for remote locations, both in the various structures of our own galaxy and in other galaxies. In this capacity red giant stars have taken on additional importance recently as a result of the discovery of a relic population in the galactic halo that are known variously as Very Metal Poor (VMP), Ultra Metal Poor (UMP), or Extremely Metal Poor (XMP) stars (Cohen *et al.* 2002). However, the derivation of chemical abundances from flux distributions and spectra is highly model dependent. Therefore, the physical realism of atmospheric models and spectrum synthesis calculations plays an important role in determining the acuity with which we can distinguish abundance patterns throughout space. The most widely used grids of models for red giant chemical abundance analyses to date have been the ATLAS series of models (Kurucz 1994) and the MARCS (most recently NMARCS) series of models (Plez *et al.* 1992). Both sets of models make use of the assumption of Local Thermodynamic Equilibrium (LTE), and the former makes use of the assumption of plane-parallel geometry. The latest LTE models have been successful at fitting the global solar flux distribution, but, it is unclear whether the expanded line lists provide a satisfactory fit to the blue and UV bands of red giant stars. Bessell *et al.* (1998) undertook a critical evaluation of how well these grids of atmospheric models fit empirical relations between stellar color and the fundamental stellar parameters of effective temperature ($T_{\rm eff}$) and bolometric magnitude ($M_{\rm bol}$). For giants of spectral types G to M, none of the models can fit the relations between $T_{\rm eff}$ and those colors that are derived from the blue or violet regions of the spectrum, such as Johnson $B-V$. They postulate that incomplete or erroneous opacity in the blue-violet region is responsible for the discrepancy. Similarly, Short & Lester (1996) found that ATLAS9 models over-predict the emergent flux by a factor of two, and systematically over-predict the strength of all spectral lines, in the violet spectral region ($\lambda \leq 4200$ Å) of red giants like Arcturus, unless the *continuous* opacity is approximately doubled, *ad hoc*.

Red giant atmospheres are relatively translucent over large path lengths and non-locally determined radiative rates often dominate collisional rates for many transitions, causing departures from local thermodynamic equilibrium (LTE). Previous investigations of exploratory scope (Gratton *et al.* 1999), (Thevenin & Idiart 1999) have found that abundances of red giant stars that are derived from *non*-LTE line profile calculations can differ significantly from those derived from LTE calculations. Furthermore, the discrepancies become larger as the metallicity is reduced to significantly sub-solar values. Therefore, *both* the atmospheric structure and the emergent spectrum should be calculated in the more general statistical equilibrium (SE), in which a set of coupled equations is solved for the rate at which

every energy level of every ionization stage of every species is populated and de-populated by various collisional and radiative processes. Given the importance to structure formation studies of chemical abundance analysis of the recently discovered XMP stars in the galactic halo, more realistic modeling of metal poor red giants is particularly important.

As a result of computational constraints, previous investigations of NLTE effects in red giant stars have treated a few chemical species in SE while treating the bulk of the strongest lines in LTE. Recently, Short *et al.* (1999) have greatly expanded the NLTE SE treatment in the general-purpose atmospheric modeling and spectrum synthesis code `PHOENIX` (Hauschildt & Baron 1999) so that over 100 000 spectral lines, including all of the strongest lines and many of the weaker lines that blanket the UV band, are now treatable in self-consistent NLTE. Even this is a small fraction of the millions of spectral lines that collectively control the emergent flux, but it is a significant step forward in improving the realism of the models. The purpose of this study is to calculate theoretical models and synthetic spectra for the mildly metal-poor standard red giant star Arcturus (α Boo, HD124897, HR5340) to assess the affect that large scale NLTE line blanketing has on the theoretical model structure and the synthetic spectrum. The modeling of a mildly metal-poor standard red giant like Arcturus with large scale SE and spherical geometry is the first step in a larger effort to model the XMP stars with unprecedented realism. In Section 2 we describe the computational modeling; in Section 3 we discuss the stellar parameters; in Section 4 we present our results for both the Sun and Arcturus, and re-iterate out main conclusions in Section 5.

2. Modeling

`PHOENIX` makes use of a fast and accurate Operator Splitting/Accelerated Lambda Iteration (OS/ALI) scheme to solve self-consistently the radiative transfer equation and the NLTE SE rate equations for many species and overlapping transitions (Hauschildt & Baron 1999). Recently Short *et al.* (1999) have greatly increased the number of species and ionization stages treated in SE by `PHOENIX` so that at least the lowest two stages of 24 elements, including the lowest six ionization stages of the 19 most important elements, are now treated in NLTE. Short *et al.* (1999) contains details of the sources of atomic data and the formulae for various atomic processes. Table 1 shows which species have been treated in NLTE in the modeling presented here, and how many E levels and $b-b$ (bound-bound) transitions are included in SE for each species. For the species treated in NLTE, only transitions of $\log gf$ value greater than -3 (designated primary transitions) are included in the SE equations. All other transitions of that species (designated secondary transitions) are treated in LTE. We

have only included in the NLTE treatment those ionization stages that are non-negligibly populated at some depth in the Sun's atmosphere. As a result, we only include the first one or two ionization stages for most elements.

Table 2 shows the six levels of realism with which we calculate our models and synthetic spectra. The six levels incorporate three degrees of realism in the treatment of the equilibrium state of the gas and the radiation field, and two degrees of realism in the geometry of the atmosphere. Unless otherwise noted, the realism of a synthetic spectrum calculation is always consistent with that of the input model used. We have investigated the behavior of NLTE models with two levels of realism: 1) NLTE treatment for H, He, and important light metals up to, but *not* including, the Fe group elements (designated $\mathrm{NLTE_{Light}}$ models), and 2) the same as the $\mathrm{NLTE_{Light}}$ models except that the Fe group elements Fe and Ti are also included in the NLTE treatment (designated $\mathrm{NLTE_{Fe}}$ models). We investigate these two levels of realism because the Fe group elements play a special role in the atmospheres and spectra of late-type stars (Thevenin & Idiart 1999); because of their spectacularly rich term structure a neutral or low ionization stage Fe group element contributes between one and two orders of magnitude more lines to the spectrum than the corresponding stage of any lighter element. Finally, we note that all of the models in Table 2 also include many tens of millions additional lines from many atoms, ions and diatomic molecules in the approximation of LTE. Hauschildt *et al.* (1999) have calculated cool super-giant models with spherical geometry and found that the broad-band emergent flux is often under-predicted by as much as 50% by plane parallel models due to the effect of sphericity on line blanketing opacity. Therefore, we include an investigation of geometry here.

3. Stellar parameters

The most recent determination of the fundamental parameters of Arcturus is that of Griffin & Lynas-Gray (1999). They compiled observations of the absolute flux distribution, F_λ, from the UV to the IR from several sources and found a total integrated flux of 4.95×10^{-5} ergs cm^{-2} s^{-1}. This they combined with a recent determination of the angular diameter, θ, by Quirrenbach *et al.* (1996) of 21.0 ± 0.2 mas to derive a $T_{\rm eff}$ value of 4291 ± 27K. They also found the closest match to their composite F_λ distribution among a grid of calculated F_λ distributions that were generated with the atmospheric models of Kurucz (1992b) and found best fit values for $T_{\rm eff}$, $\log g$, and [A/H] of 4291.9 ± 0.7K, 1.94 ± 0.05, and -0.68 ± 0.02. The close agreement between the $T_{\rm eff}$ values determined from two independent methods is reassuring, and both the $T_{\rm eff}$ value and the $\log g$ value are within the range of most

previous determinations. Their value of [A/H] is near the lower end of the range of previously determined values.

A recent thorough determination of the parameters using another technique, LTE spectral fitting of the profiles of many lines throughout the visible band, by Peterson *et al.* (1993), yielded the values $T_{\rm eff} = 4300 \pm 30$K, $\log g = 1.5 \pm 0.15$, and a value [A/H] $= -0.5 \pm 0.1$ for most elements, with α-process elements twice as abundant. The $T_{\rm eff}$ value of the latter study is in very close agreement with both values derived by Griffin & Lynas-Gray (1999), has a $\log g$ value near the lower end of the generally accepted range for Arcturus, is more metal rich by 0.2 dex, and has a non-solar abundance pattern.

Decin *et al.* (2000), Decin *et al.* (2003b) and Decin *et al.* (2003a) have fit synthetic spectra based on plane-parallel and spherical LTE atmospheric models to the near IR band (2.38 to 4.08 μm) as observed by the Short-Wavelength Spectrometers of the Infrared Space Observatory (ISO-SWS) for a wide range of late-type giant stars, including Arcturus. Their modeling was part of a program to simultaneously investigate the calibration of ISO-SWS and the realism of atmospheric models. Therefore, they performed a thorough analysis of the dependence of the strength of individual molecular features throughout the 2.38 to 4.08 μm band on the value of individual stellar parameters. Decin *et al.* (2003a) find the following best fit parameters: $T_{\rm eff} = 4320 \pm 140$ K, $\log g = 1.50 \pm 0.15$, [A/H] $= -0.5 \pm 0.20$, and $\xi_{\rm t} = 1.7 \pm 0.5$ km s^{-1}. They also found that C/Fe, N/Fe, and O/Fe are enhanced by 0.1, 0.4, and 0.4, respectively, with respect to the solar ratios. The values of $T_{\rm eff}$ and [A/H] are in agreement, to within the uncertainties, of both Griffin & Lynas-Gray (1999) and Peterson *et al.* (1993), and the $\log g$ value agrees with that of Peterson *et al.* (1993).

Because Arcturus is a thick disk population (mildly Population II) star, one may expect a non-solar abundance distribution such as that reported by Peterson *et al.* (1993) and Decin *et al.* (2003a). Indeed, the possibility of detecting such a pattern by way of accurate modeling and spectrum synthesis is important in the broader context of galactic chemical evolution, and is the motivation for the improved modeling presented here. However, our purpose in this initial assessment of the massively NLTE models is to investigate the extent to which the incorporation of NLTE effects for most of the strong atomic lines affects the calculated equilibrium model structure and emergent F_λ distribution. To that end we adopt a canonical model with a scaled solar abundance distribution, designated T43G20M07, with the parameters of Griffin & Lynas-Gray (1999), rounded to the nearest cardinal values typically used in model atmosphere grids: $T_{\rm eff} = 4300$K, $\log g = 2.0$, and [A/H] $= -0.7$. For

exploratory purposes we also study four models at adjacent points that span the range of values in $T_{\rm eff}$, $\log g$, and [A/H] that have been found by various investigators. Table 3 displays the model designations and parameters for this small grid. T43G15M07, T43G20M04, T43G15M04, and T42G20M07.

Unique specification of a spherical model requires a parameter in addition to $T_{\rm eff}$, $\log g$, and [A/H]. We set the radius at a standard optical depth of unity $R(\tau_{12000} = 1)$ equal to $23{\rm R}_\odot$ in keeping with the value that Griffin & Lynas-Gray (1999) found from fitting the overall flux distribution and the measured angular diameter. The specification of $\log g$ and R sets the mass, M, by way of the formula for surface gravity, $g = GM/R^2$, to $2{\rm M}_\odot$. The specification of $T_{\rm eff}$ and R sets the bolometric luminosity, $L_{\rm Bol}$, to $4\pi R^2 \sigma T_{\rm eff}^4$ (by the definition of $T_{\rm eff}$), which is 160 $\rm L_\odot$ ($M = -0.7$). By comparison, Decin *et al.* (2003a) used the same relations with their best-fit stellar parameters to find: $R(\tau_{\rm Continuum} = 1) = 25.06 \pm 1.56{\rm R}_\odot$, $M = 0.75 \pm 0.27{\rm M}_\odot$, and $L = 197 \pm 36{\rm L}_\odot$. Their lower value of M is consistent with the lower value of $\log g$ that they adopted. We adopt a depth-constant micro-turbulent velocity dispersion, $\xi_{\rm T}$, of 2.0 km $\rm s^{-1}$.

4. Results

4.1. Model structure

Fig. 1 shows the computed kinetic temperature ($T_{\rm kin}$) structure for the canonical Arcturus models (T43G20M07) with the different levels of physical realism. We use the LTE PP model as a reference model for the comparison in the lower panel. The atmosphere is sufficiently extended compared to the radius of the star that the effects of sphericity are significant. Especially interesting is the dependence of the sphericity effect on the extent to which the model deviates from LTE. Comparing the dashed lines in Fig. 1 we see a trend of increasing surface cooling with increasing NLTE effects among the PP models. The PP $\rm NLTE_{Light}$ and $\rm NLTE_{Fe}$ models are cooler than the PP LTE model by more than 50 and 250K at the top of the atmosphere, respectively. By contrast, comparing the solid lines we see that the spherical $\rm NLTE_{Light}$ model deviates negligibly ($\leq$ 10K) from the spherical LTE model. As a result, with PP modeling one would overestimate the effect of NLTE among light metals on the model structure. Both the spherical LTE and spherical $\rm NLTE_{Fe}$ models are about 50K warmer near the top of the atmosphere than their LTE counterparts, so among the spherical models the $\rm NLTE_{Fe}$ is still about 250K cooler than the LTE model. In every case, spherical models are always warmer throughout the outer atmosphere than PP models. In their study of sphericity effects in line blanketed giants and super-giants,

Hauschildt *et al.* (1999) also found that spherical models were warmer than corresponding PP models (see their Fig. 8).

4.2. Absolute flux distribution

Fig. 2 shows the overall F_λ distribution of the canonical model (T43G20M07) calculated with all levels of physical realism, diluted to the distance of Arcturus using the measured angular diameter of 21.0 mas (Quirrenbach *et al.* 1996). The observed F_λ distributions are that of Alekseeva *et al.* (1996) and Breger (1976). The computed distributions have a spectral resolution, R, of 50 000 and we have convolved them with a Gaussian of FWHM equal to 50Å to match the sampling of the Alekseeva *et al.* (1996) data. We also show the difference between the various computed F_λ distributions and the observed distribution as a percentage of the observed distribution. All computed distributions are in general agreement with the over-all flux level in the red and yellow bands of the Alekseeva *et al.* (1996) short wavelength data-set. However, all over-predict the flux by as much as 150% with decreasing λ into the blue and UV bands. The spherical models have less flux than the PP models by as much as 10% throughout the blue and UV, thereby providing a fit that is marginally closer, but still poor.

The LTE and $\mathrm{NLTE_{Fe}}$ models differ negligibly from each other for $\lambda > 5000$Å, but for shorter λ values the $\mathrm{NLTE_{Fe}}$ model becomes increasingly brighter than the LTE model. As a result, with these stellar parameters the LTE model provides a marginally closer fit to the observed F_λ level than the more realistic $\mathrm{NLTE_{Fe}}$ model.

The reason for the increased F_λ level in the UV with the $\mathrm{NLTE_{Fe}}$ model can be seen in Figs. 3 and 4. Because of its rich term structure, Fe contributes a significant fraction of the total line opacity, particularly in the UV band. Although the Fe I b_i values are larger than unity for many of the higher E levels in the outermost part of the atmosphere, the ground state and all the lower E levels are under-populated with respect to LTE. This is due to an over-ionization of Fe with respect to LTE that depletes the Fe I population throughout the atmosphere. As a result, the veil of Fe opacity in the UV band is weakened which allows more flux to escape in the UV.

We re-emphasize that our calculations are carried out using the the expanded line list of Kurucz (1992a), which was found to provide a close fit the the UV flux level of the Sun.

Apparently, the ability of the expanded line list to address the solar UV flux problem does not extend to all red giants. Given the magnitude of the differences in the $T_{\rm kin}$ structure of the outermost depths between the LTE and NLTE models, seen in Fig. 1, we have also performed an internally inconsistent calculation of the F_λ distribution with the $\rm NLTE_{Fe}$ set-up using the LTE model as input. This F_λ distribution lies very close to that of the self- consistent $\rm NLTE_{Fe}$ calculation, which indicates that the direct effects of NLTE radiative transfer and statistical equilibrium are a much larger influence on the spectrum formation than the effect of NLTE atmospheric structure. Given the agreement between the LTE and NLTE models at deeper layers around $\tau_{12000} = 1$, the relative unimportance of the atmospheric structure in determining the emergent F_λ is not surprising.

Excess model flux in the UV suggests that the $T_{\rm eff}$ value of the model (4300K) may be too high, although the range of recent determination from a variety of methods is constrained to within 50K. Furthermore, previous $\log g$ and [A/H] determinations have ranged from our values of 2.0 and -0.7 to 1.5 and -0.4. To test whether NLTE models provide a better fit with other values within the error range of the stellar parameters, we converged a small grid of four spherical LTE and $\rm NLTE_{Fe}$ models in the $\log g - $ [A/H] plane, all with a $T_{\rm eff}$ value of 4300K. The grid is displayed in Table 3. Furthermore, we converged spherical LTE and $\rm NLTE_{Fe}$ models with a $T_{\rm eff}$ value of 4200K and our canonical $\log g$ and [A/H] values of 2.0 and -0.7. The latter model is well outside the error limit of recent $T_{\rm eff}$ determinations, but we include it to demonstrate by how much $T_{\rm eff}$ must deviate from the canonical value to force a fit to the UV flux level.

Fig. 5 shows the comparison among synthetic F_λ distributions of spherical LTE and $\rm NLTE_{Fe}$ models in the $\log g - $ [A/H] grid. All models provide F_λ distributions that agree relatively closely for $\lambda > 5000$ Å, and become increasingly distinct from each other as λ decreases. Both the decrease in $\log g$ and the increase in [A/H] serve to decrease the predicted UV band F_λ level. The latter effect is expected due to the increase in line blanketing with decreasing λ. There is an approximate "degeneracy" in $\log g$ and [A/H] in that the T43G15M07 and T43G20M04 models give rise to UV F_λ levels that are barely distinguishable. Our calculations allow us to assess the dependency of the magnitude of NLTE effects on the stellar parameters. The extent of the NLTE UV brightening due to Fe over-ionization is sensitive to [A/H], but not to $\log g$. The amount of NLTE UV brightening is as much as 10% greater in the models of [A/H] = 0.4 than it is in models of [A/H] = 0.7. Therefore, we find, for this metallicity range, that the effect of NLTE on the overall UV flux level *decreases* with decreasing metallicity.

Fig. 6 shows the comparison of synthetic F_λ distributions of spherical NLTE$_{\rm Fe}$ models in the $\log g - [{\rm A/H}]$ grid and of the $T_{\rm eff} = 4200$K model to the observed spectrum. All models provide approximately the same quality of fit to the observed F_λ distribution throughout the yellow and red bands. Even the model that is faintest in the UV, T43G15M04, is as much as 100% too bright between 3000 and 3500 Å. Therefore, throughout the $\log g - [{\rm A/H}]$ range in which Arcturus is expected to lie, no model of $T_{\rm eff} = 4300$K provides even an approximately close match to the observed blue and UV brightness. The 4200K model provides a closer match to the overall observed UV F_λ level, but is systematically too faint throughout the visible band where $F_\lambda(\lambda)$ peaks and the Rayleigh-Jeans tail begins. We conclude that the UV discrepancy is not due to incorrect values of the stellar parameters.

It should be noted that, generally, for late-type stars, F_λ in the mid to far UV bands exceeds the values predicted by models in radiative and convective equilibrium because in these bands the flux arises from layers above the temperature minimum region where the temperature distribution with depth is inverted due to the presence of a chromosphere. However, this extra flux due to non-radiative heating of the outer atmosphere typically arises only in the $\lambda < 2500$Å region (Morossi *et al.* 1993). Therefore, the presence of a chromosphere is not likely to be the cause of the blue and near UV band discrepancy found in K2 III stars.

4.3. Comparison to other late-type giants

A potentially important clue as to the nature of the blue/near-UV band discrepancy is its variation with stellar parameters. We have computed spherical LTE models for four late-type giants for which we found reliable stellar parameters compiled in Morossi *et al.* (1993) and spectrophotometric data in the catalogues of Alekseeva *et al.* (1996) or Burnashev (1985). The Morossi *et al.* (1993) list only contains stars of $[{\rm A/H}] \approx 0$ with a quoted uncertainty of ± 0.25, so they are more metal rich than Arcturus. The stars span a range in spectral type from late G to mid K, but are all within four spectral sub-types of Arcturus, and a range in luminosity class from sub-giant to bright giant. HR165 is almost an exact Arcturus analogue, but has a higher metallicity than Arcturus. Details of the stars and spectrophotometric data sources are presented in Table 5, and the comparison of observed and theoretical spectra is shown in Fig. 7. Because the purpose of these comparisons is to investigate the goodness of fit in the blue and near UV band with respect to that in the red band, we arbitrarily scaled all spectra to produce an average flux level of unity in the 7000 to 7400 Å band.

For HR165 (K3 III), HR6869 (G8 IV) and HR6705 (K5 III), theoretical spectra that are force fit to the observed spectra in the red provide a very close match to the observed spectrum throughout the blue and near UV bands. This result suggests that the blue and near UV band discrepancy is metallicity dependent in that mildly metal poor red giants like Arcturus generally exhibit the discrepancy, whereas solar metallicity red giants do not (Fig. 7). Such a metallicity dependent UV band flux discrepancy suggests NLTE effects as the cause, but, as can be seen from Fig. 2, NLTE effects make the discrepancy *worse*. Note that spherical *NLTE* models may not necessarily fit these solar metallicity stars as well as spherical LTE models do; our conclusions are based on a *differential* assessment of the fit provided by LTE models to mildly metal poor stars on one hand, and to solar metallicity stars on the other hand.

4.4. UV opacity

The prediction of too much flux in the near UV band of Arcturus was also found by Short & Lester (1996) on the basis of PP LTE modeling with the ATLAS9 code of (Kurucz 1992a) and SPECSYN LTE spectrum synthesis code of Kurucz & Avrett (1981). There has been much discussion of "missing UV opacity" in the models of the Sun (see Kurucz (1990), Kurucz (1992a) for example), and Kurucz (1992a) achieved the first close fit to the *solar* UV flux level at low resolution by incorporating the opacity of tens of millions of new theoretically predicted atomic lines. Short & Lester (1996) suggested that the discrepancy may be due to the presence of an unknown source of *continuous absorption* opacity, $\kappa_{\rm Cnt}$, in the star that is unaccounted for in the atmospheric model. They doubled the amount of violet and near UV band continuous opacity in their red giant model, *ad hoc*, and showed that the additional opacity lowered the predicted violet F_λ such that it provided a much closer match to the observed F_λ level. Short & Lester (1996) also showed the addition of extra opacity in the region below 4000Å had no significant effect on the equilibrium structure of the atmosphere because most of the flux is at longer λ values. A limitation of the Short & Lester (1996) study was the use of PP LTE models. However, the more realistic models presented here over-predict the blue and near UV flux by *even more* than the LTE PP models. *Therefore, the more realistic models in no way address the UV flux problem for red giants, and do not obviate the need for increased opacity that was suggested by Short & Lester (1996).*

5. Conclusions

We have presented atmospheric models and synthetic flux spectra for the red giant star Arcturus that represent two degrees of realism in the treatment of the atmospheric geometry and three degrees of realism in the treatment of the equilibrium state of the gas and the radiation field. We have studied the ability of these models to fit the overall absolute $F_\lambda(\lambda)$ level. We find that NLTE over-ionization of Fe I substantially reduces the UV line opacity and allows more flux to escape there. NLTE models predict approximately 50% greater flux in the blue and near UV band than LTE models. Both LTE and NLTE models predict as much as 100 to 150% larger flux than observed in the blue and near UV flux bands This excess of model UV flux may indicate that there is *still* substantial UV opacity missing from the models, despite the greatly expanded line lists of Kurucz (1992a). The extent of the UV excess depends on whether the Fe group elements are treated in NLTE. Also, we find that for the [A/Fe] range -0.4 to -0.7 the effect of NLTE on the overall UV flux level *decreases* with decreasing metallicity.

We calculated spherical LTE models for late G and early to mid-K giants of *solar* metallicity with reliable stellar parameters, and found that they generally provided a close match to the observed flux distributions for such stars from the near IR to the near UV band. Therefore, the blue/near-UV discrepancy is likely metallicity dependent in the sense that it increases with decreasing metallicity. Such a metallicity dependent flux discrepancy between observed and modeled flux distributions suggests that NLTE effects are the cause. However, we find that treating a large amount of the line opacity in self-consistent NLTE *increases* the size of the discrepancy.

5.1. Future work

Given the results presented here, we are currently working on expanding our $\mathrm{NLTE_{Fe}}$ calculations to span a range of stellar parameter space among late G and early K giants. Our goal is to map out in more detail the metallicity dependency of the blue/near-UV flux discrepancy by applying NLTE models with the highest level of realism to all such stars with observed global flux distributions. The satisfactory resolution of this discrepancy is necessary for accurate modeling of the recently discovered XMP stars.

CIS gratefully acknowledges funding from Saint Mary's University and from the Charles E. Schmidt College of Science at Florida Atlantic University. This work was supported in

part by NSF grant AST-9720704, NASA ATP grant NAG 5-8425 and LTSA grant NAG 5-3619 to the University of Georgia. PHH was supported in part by the Pôle Scientifique de Modélisation Numérique at ENS-Lyon. Some of the calculations presented in this paper were performed at the San Diego Supercomputer Center (SDSC), supported by the NSF, on the IBM pSeries 690 of the Norddeutscher Verbund für Hoch- und Höchstleistungsrechnen (HLRN), and at the National Energy Research Supercomputer Center (NERSC), supported by the U.S. DOE. We thank all of these institutions for a generous allocation of computer time.

REFERENCES

Alekseeva G.A., Arkharov A.A. , Galkin V.D. , Hagen-Thorn E.I., Nikanorova I.N., Novikov V.V., Novopashenny V.B., Pakhomov V.P., Ruban E.V., Shchegolev D.E., 1997, *Baltic Astron.*, 5, 603

Bell R.A., Paltoglou G., Tripicco M.J., 1994, MNRAS, 268, 771

Bessell, M. S., Castelli, F., Plez, B., 1998, A&A, 333, 231

Breger M., 1976, ApJS, 32, 7

Burnashev V.I., 1985, Abastumanskaya Astrofiz. Obs. Bull. 59, 83

Cohen, J.G., Christlieb, N, Beers, T.C., Gratton, R., Carretta, E., 2002, ApJ, 124, 470

Decin, L., Vandenbussche, B., Waelkens, C., Decin, G., Eriksson, K., Gustafsson, B., Plez, B., Sauval, A. J., 2003, A&A, 400, 709

Decin, L., Vandenbussche, B., Waelkens, C., Eriksson, K., Gustafsson, B., Plez, B., Sauval, A.J., Hinkle, K., 2003, A&A, 400, 679

Decin, L., Waelkens, C., Eriksson, K., Gustafsson, B., Plez, B., Sauval, A.J., Van Assche, W., Vandenbussche, B., 2000, A&A, 364, 137

Gratton, R. G., Carretta, E., Eriksson, K., Gustafsson, B., 1999, A&A, 350, 955

Griffin, R., 1968, A photometric atlas of the spectrum of Arcturus, Cambridge: Cambridge Philosophical Society

Griffin, R. E. M., Lynas-Gray, A. E., 1999, AJ, 117, 2998

Hauschildt, P. H., Allard, F., Ferguson, J., Baron, E., Alexander, D. R., 1999, ApJ, 525, 871

Hauschildt, P.H. and Baron, E., 1999, J. Comp. App. Math., 109, 41

Kurucz R.L. 1994, CD-ROM No 19

Kurucz, R.L., 1992, Rev. Mex. Astron. Astrofis., 23, 181

Kurucz, R.L., 1992, in The Stellar Populations of Galaxies, ed. B. Barbuy & A. Renzini (Dordrecht: Reidel), 225

Kurucz, R.L. 1990, Trans. IAU, XXB 168

Kurucz, Robert L., Avrett, Eugene H., 1981, SAO Special Report 391

Morossi, C., Franchini, M., Malagnini, M. L., Kurucz, R. L., Buser, R., 1993, A&A, 277, 173

Peterson, R.C., Dalle Ore, C.M., Kurucz, R.L., 1993, ApJ, 404, 333

Plez, B., Brett, J. M., Nordlund, A., 1992, A&A, 256, 551

Quirrenbach, A., Mozurkewich, D., Buscher, D.F., Hummel, C.A., Armstrong, J.T., A&A, 312, 160

Short, C. I., Hauschildt, P. H., Baron, E., 1999, ApJ, 525, 375

Short, C. I., Lester, J. B., 1996, ApJ, 469, 898

Thevenin, F. & Idiart, T.P., 1999, ApJ, 521, 753

Table 1. Species treated in Non-Local Thermodynamic Equilibrium (NLTE) in the $NLTE_{Light}$ and $NLTE_{Fe}$ models. Each ionization stage is labeled with the number of energy levels and bound-bound transitions included in the statistical equilibrium rate equations. Note that this table shows only a sub-set of the total number of species that are currently treatable in statistical equilibrium by Phoenix.

Element	Model	Ionization Stage		
		I	II	III
H	$NLTE_{Light}$, $NLTE_{Fe}$	*80/3160*	···	···
He	$NLTE_{Light}$, $NLTE_{Fe}$	19/37	···	···
Li	$NLTE_{Light}$, $NLTE_{Fe}$	57/333	55/124	···
C	$NLTE_{Light}$, $NLTE_{Fe}$	228/1387	···	···
N	$NLTE_{Light}$, $NLTE_{Fe}$	252/2313	···	···
O	$NLTE_{Light}$, $NLTE_{Fe}$	36/66	···	···
Ne	$NLTE_{Light}$, $NLTE_{Fe}$	26/37	···	···
Na	$NLTE_{Light}$, $NLTE_{Fe}$	**53/142**	35/171	···
Mg	$NLTE_{Light}$, $NLTE_{Fe}$	**273/835**	72/340	···
Al	$NLTE_{Light}$, $NLTE_{Fe}$	**111/250**	**188/1674**	···
Si	$NLTE_{Light}$, $NLTE_{Fe}$	329/1871	93/436	···
P	$NLTE_{Light}$, $NLTE_{Fe}$	**229/903**	**89/760**	···
S	$NLTE_{Light}$, $NLTE_{Fe}$	146/439	84/444	···
K	$NLTE_{Light}$, $NLTE_{Fe}$	**73/210**	**22/66**	···
Ca	$NLTE_{Light}$, $NLTE_{Fe}$	194/1029	87/455	150/1661
Ti	$NLTE_{Fe}$	395/5279	204/2399	···
Fe	$NLTE_{Fe}$	494/6903	617/13675	···

Note. — Elements in bold face have been added since the last NLTE `PHOENIX` modeling of red giant stars. Those in italics have had their treatment improved since the last modeling.

Table 2: Levels of modeling realism.

Degree of NLTE	Geometry	
	Plane-Parallel	Spherical
None	LTE(PP)	LTE
Light metals only	$\mathrm{NLTE_{Light}}(PP)$	$\mathrm{NLTE_{Light}}$
Light metals & Fe+Ti	$\mathrm{NLTE_{Fe}}(PP)$	$\mathrm{NLTE_{Fe}}$

Table 3: Model grid.

Designation	$T_{\rm eff}$	$\log g$	[A/H]
T43G20M07[a]	4300	2.0	-0.7
T43G15M07	4300	1.5	-0.7
T43G20M04	4300	2.0	-0.4
T43G15M04	4300	1.5	-0.4
T42G20M07	4200	2.0	-0.7

[a]Canonical model

Table 4: Pulkovo Spectrophotometric Catalogue stars that are Arcturus analogues.

HR number	Flamsteed	Spectral type
2260		K3 III
4232	ν Hya	K2 III
4630	ϵ Crv	K2.5 IIIa
6223	18 Dra	K0 III
6859	δ Sgr	K3 IIIa

Table 5: Late-type giant stars of [A/H] = 0.0 with reliable parameters (Morossi *et al.* 1993).

HR number	Flamsteed	Spectral type	$T_{\rm eff}$	$\log g$	Data source
165	δ And	K3 III	4300	2.0	Alekseeva *et al.* (1996)
6705	γ Dra	K5 III	3900	1.5	Alekseeva *et al.* (1996)
6869	η Ser	G8IV	4900	3.0	Alekseeva *et al.* (1996)

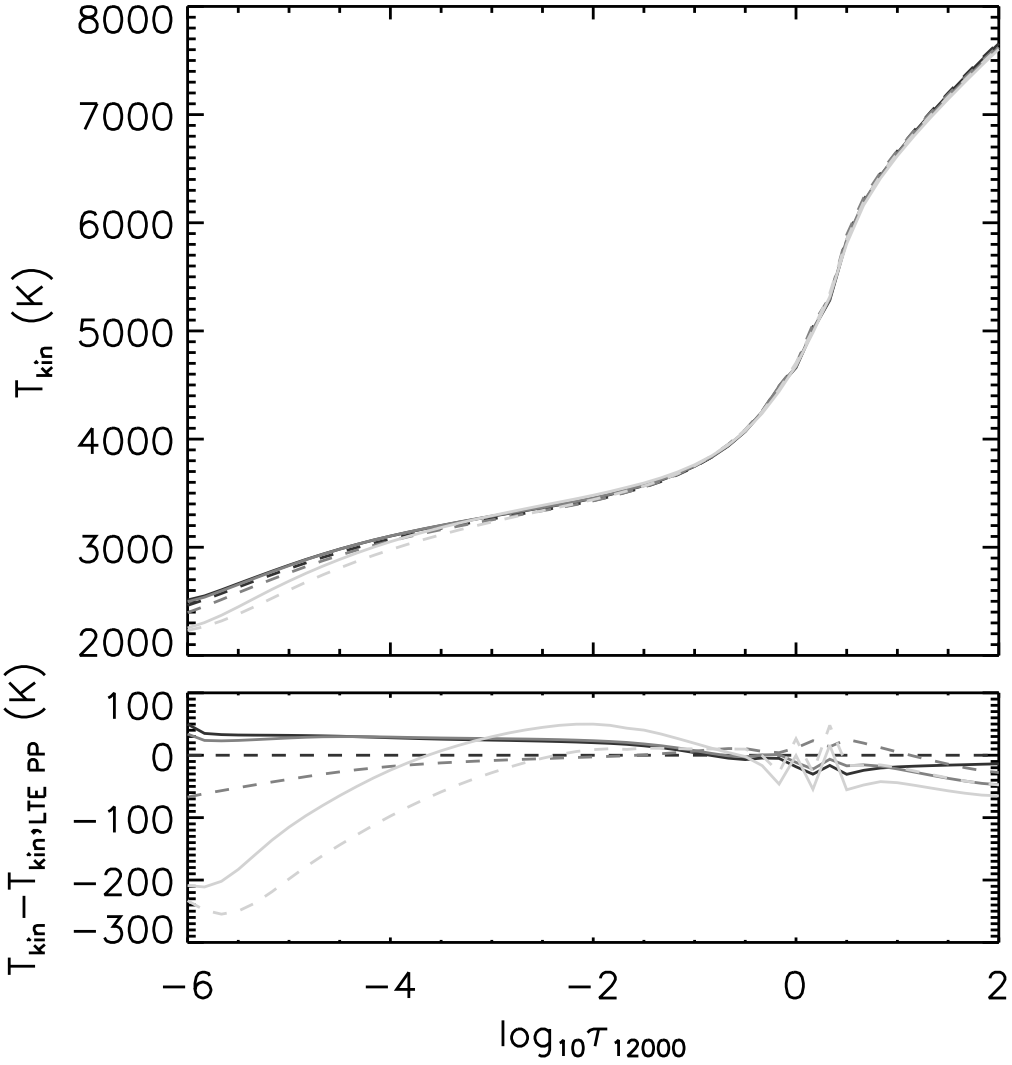

Fig. 1.— Temperature ($T_{\rm kin}$) structure of theoretical atmospheric models of Arcturus computed with: LTE (dark lines), light metals in NLTE ($\rm NLTE_{Light}$) (medium lines), light metals and Fe and Ti in NLTE ($\rm NLTE_{Fe}$) (light lines). For each degree of NLTE, the models were computed with spherical geometry (solid lines) and plane-parallel (PP) geometry (dashed lines). Upper panel: Absolute $T_{\rm kin}$, lower panel: $T_{\rm kin}$ relative to that of the LTE PP model.

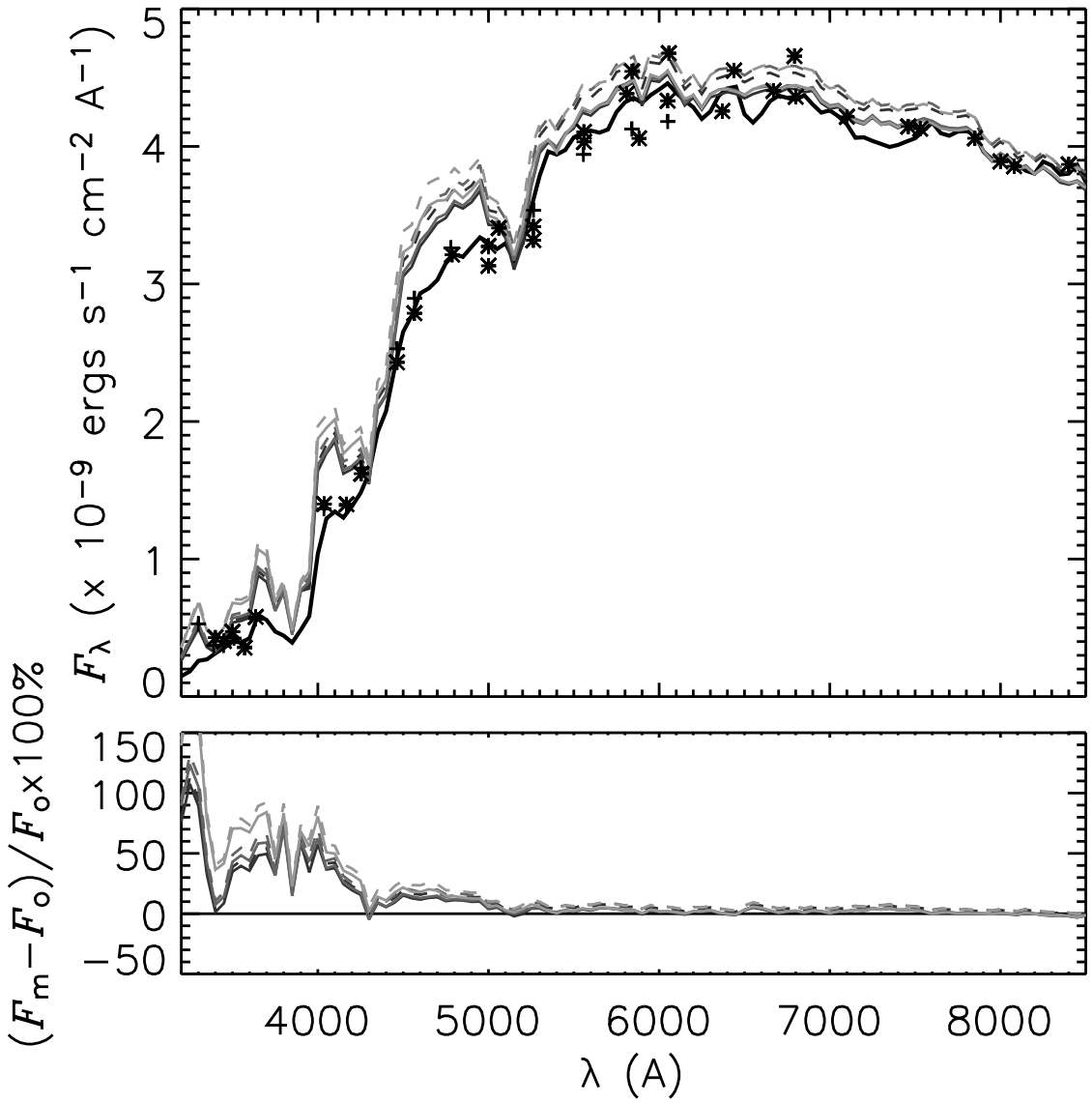

Fig. 2.— Comparison of the observed (thick black line) and computed $F_\lambda(\lambda)$ distribution. The asterisks are intermediate band spectrophotometry from Breger (1976). Computed distributions are shown for models calculated in PP (dashed lines) and spherical (solid lines) geometry for the LTE (dark thin line), $\mathrm{NLTE_{Light}}$ (medium line), and $\mathrm{NLTE_{Fe}}$ (light line) models. Upper panel: Absolute F_λ, lower panel: the difference between the model (F_m) and observed (F_o) F_λ distributions, as a percentage of observed F_λ.

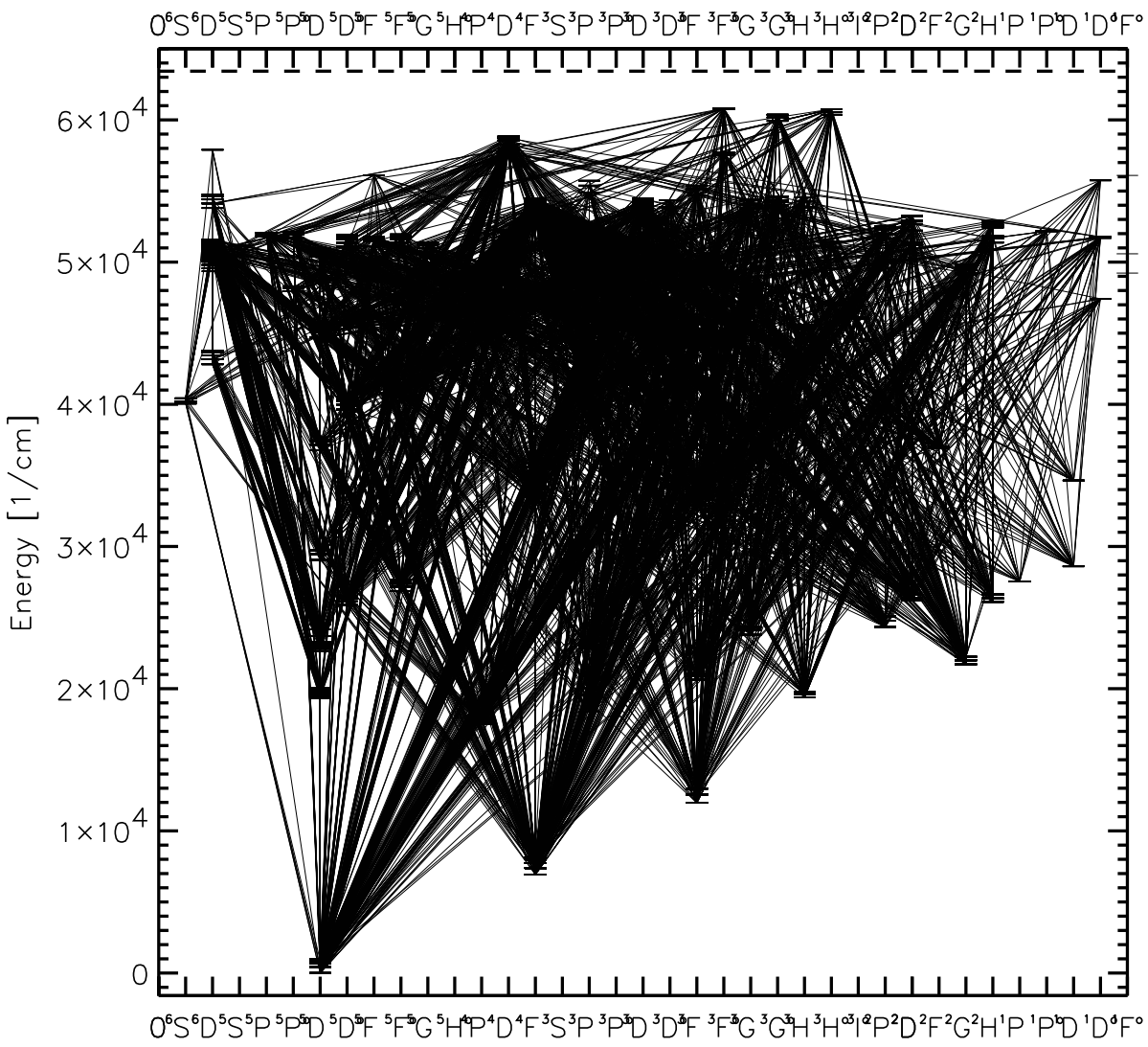

Fig. 3.— Grotrian diagram of the model Fe I atom used in our NLTE calculations.

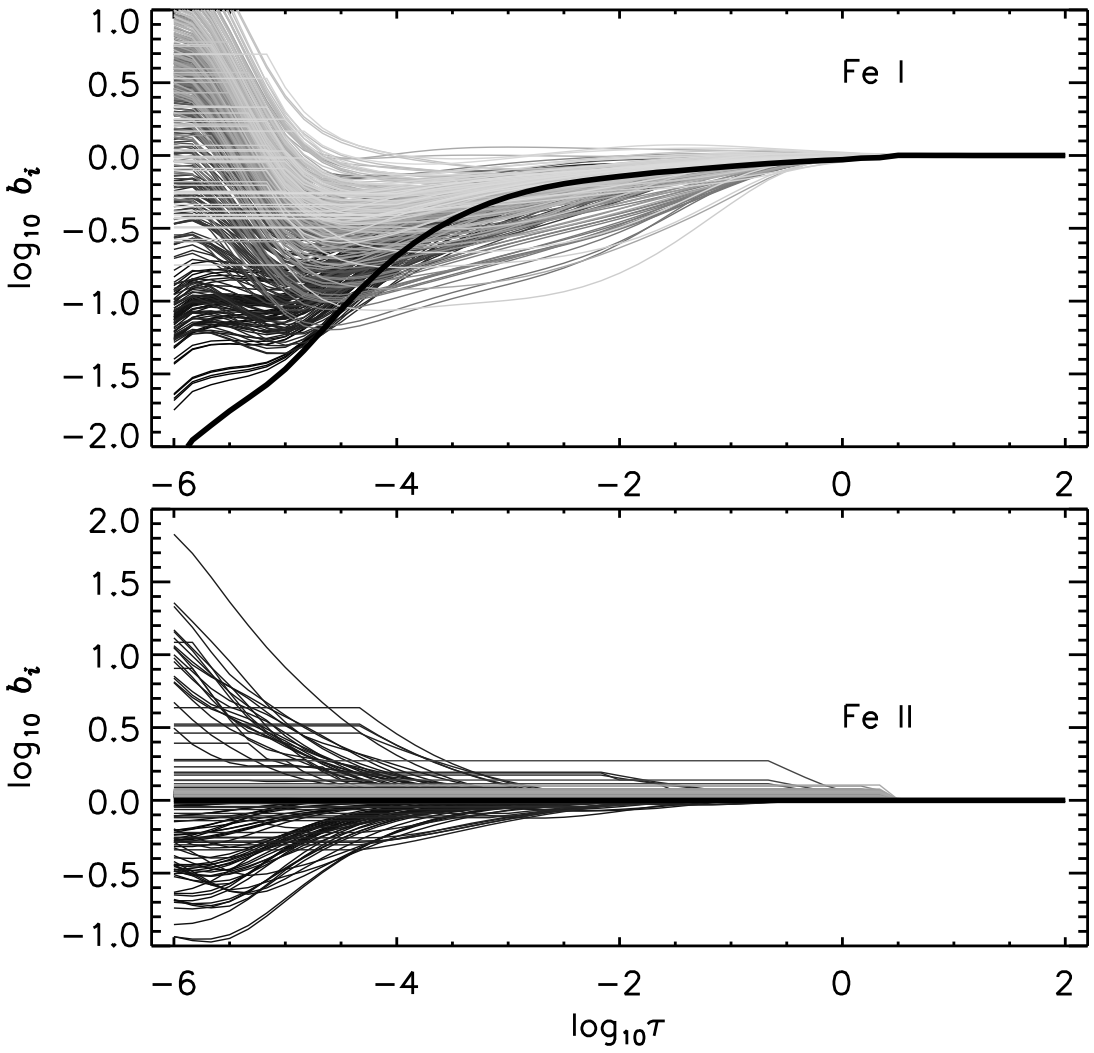

Fig. 4.— NLTE departure coefficients for Fe I and II in the $\mathrm{NLTE_{Fe}}$ model of Arcturus. The ground state coefficient is shown with a thick black line. The lighter the color of the line the higher the energy, E, of the level.

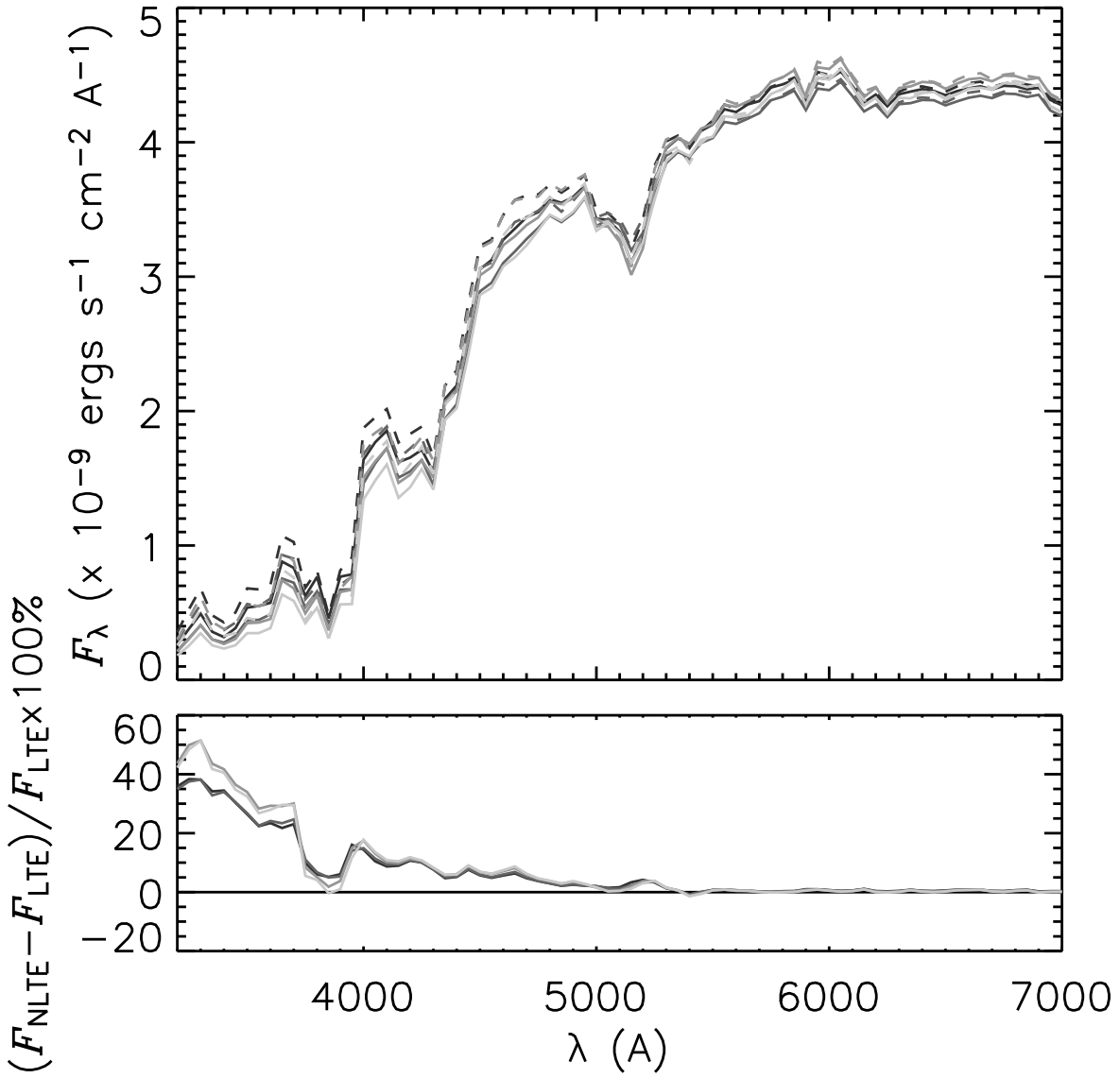

Fig. 5.— Comparison among computed $F_\lambda(\lambda)$ distributions for the spherical LTE and $\mathrm{NLTE_{Fe}}$ models throughout the parameter grid. In order of decreasing line darkness, T43G20M07 (canonical parameters), T43G15M07, T43G20M04, and T43G15M04. Solid lines: LTE models; dashed lines: $\mathrm{NLTE_{Fe}}$ models. Upper panel: Absolute F_λ distributions; lower panel: difference between NLTE and LTE models for each set of stellar parameters.

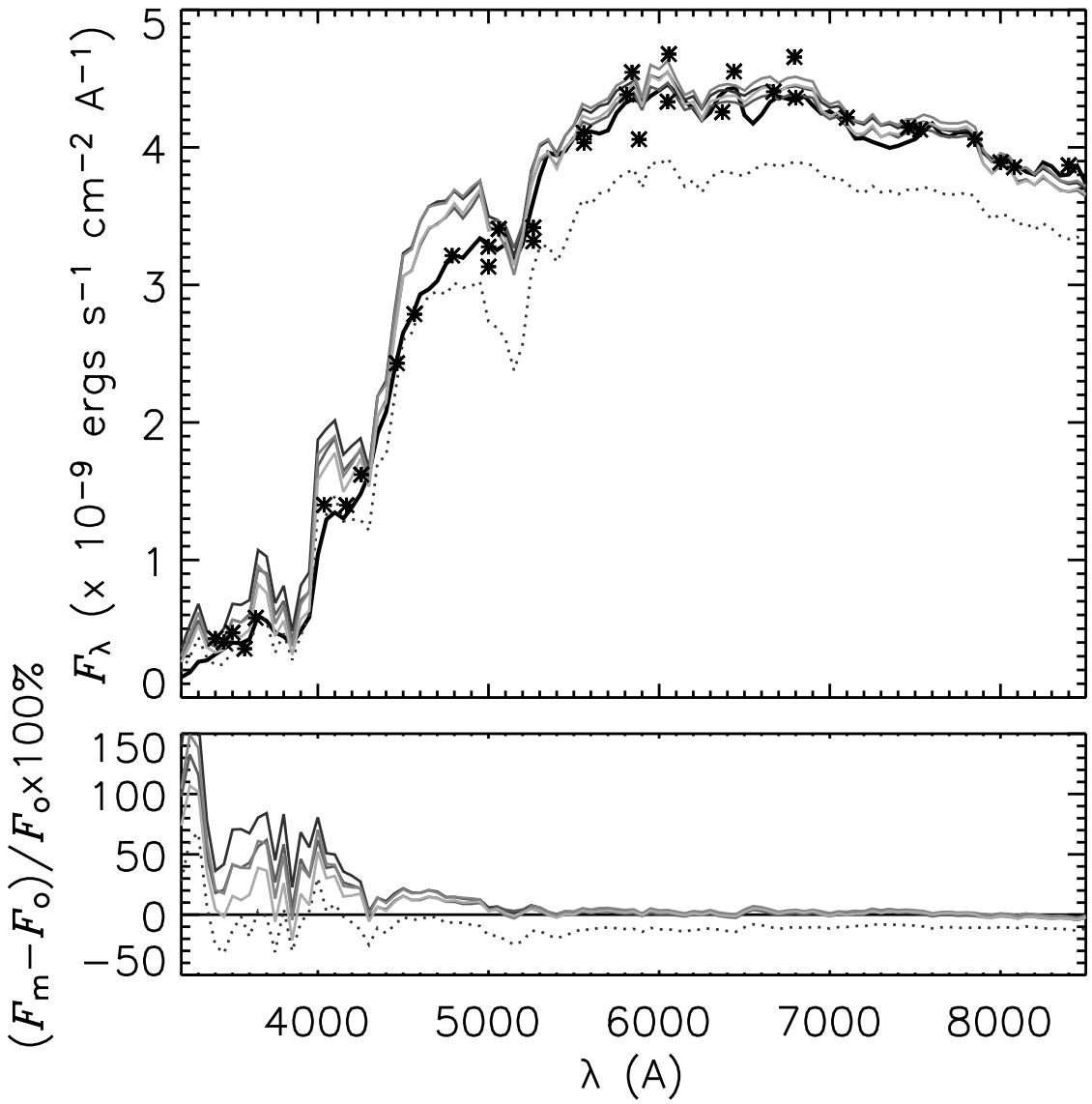

Fig. 6.— Comparison of observed and computed $F_\lambda(\lambda)$ distributions for models throughout the parameter grid. Observed spectrum: thick black line. Theoretical distributions are shown for the spherical NLTE$_{\rm Fe}$ models, in order of decreasing line darkness, T43G20M07 (canonical parameters), T43G15M07, T43G20M04, and T43G15M04; dotted line: T42G20M07. Upper panel: Absolute F_λ, lower panel: the difference between the model ($F_{\rm m}$) and observed ($F_{\rm o}$) F_λ distributions, as a percentage of observed F_λ.

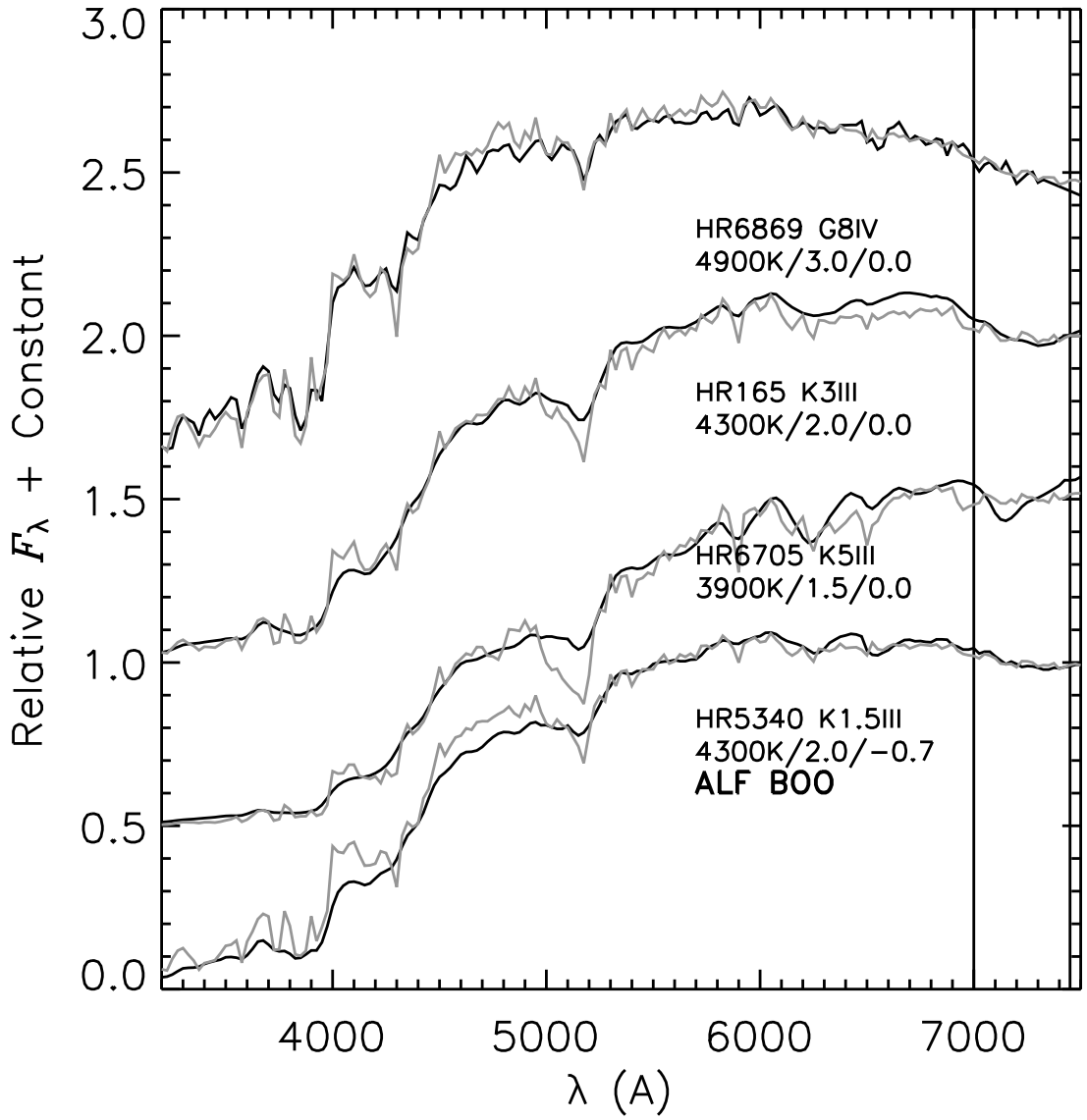

Fig. 7.— Comparison of observed and $F_\lambda(\lambda)$ distributions to theoretical distributions computed with spherical LTE models for a sample of late-type giant stars with reliable stellar parameters from Morossi *et al.* (1993) (details in Table 5). Spectrophotometric data for all stars are from Alekseeva *et al.* (1996) Observed and computed spectra are rectified to a mean flux value of unity in the 7000 to 7450Åband (vertical lines).